Smartrock transport during snowmelt floods: Discharge controls on rest scaling from seconds to seasons

Kealie L. G. Pretzlav[1,*], Joel P. L. Johnson [1,†], D. Nathan Bradley[2]

[1] Dept. of Geological Sciences, The University of Texas at Austin, Austin, TX, USA

[2] U.S. Bureau of Reclamation, Denver, CO, USA, ORCID 0000-0003-3062-9494

*Now at Balance Hydrologics, Berkeley, CA, USA, ORCID 0000-0002-9917-7206

[†]Corresponding author, joelj@jsg.utexas.edu, ORCID 0000-0001-6286-9949

Abstract

We quantify how changes in natural flood discharge control bedload rest time distributions and may influence particle diffusion through mountain river networks. We embedded accelerometers and gyroscopes into artificial cobbles deployed in Halfmoon Creek, Colorado, USA, and measured bedload transport during 28 daily snowmelt flood hydrographs in 2015. From the motion sensor data we calculate motion and rest distributions over ≈6 orders of temporal magnitude, from ≈2 seconds to ≈1 month. Motion durations follow a thin-tailed exponential distribution. Rests > 12 hours can be well fit by both truncated Pareto distributions and exponentially-tempered Pareto distributions, suggesting ambiguity in whether rests remain heavy-tailed or transition to thin tails at even longer timescales. Rest time scaling varies not only with timescale but also with flow intensity, becoming less heavy-tailed as shear stress increases. A rest time scaling break at ≈12 hours may be caused by daily discharge cyclicity.

Plain language summary

Gravel moves downstream during floods in mountain streams. Some grains move faster and farther and some move slower and shorter distances, causing sediment to spread out along channels over time. Predicting this spreading—called diffusion—is useful for understanding effects of floods along rivers, including patterns of erosion and deposition. We used "smartrocks" containing accelerometers and batteries to measure exactly when individual sediment grains moved during a month-long flood in the Rocky Mountains of Colorado. The data were used to calibrate various equations that relate movements to diffusion. These equations can improve predictions of how different floods will cause gravel to spread downstream during future floods.

Key Points

- Sensor-embedded cobble tracers quantify rest and hop durations during snowmelt-driven bedload transport in a natural mountain stream.
- Cobble rest time scaling varies with hydraulic forcing as well as with timescale.
- Heavy-tailed rests and thin-tailed hop durations imply a transition from subdiffusion to superdiffusion with increases in both timescale and shear stress.

1. Introduction

Understanding how hydrologic forcing controls sediment advection and diffusion during floods is important for improving predictions of bedload transport and channel evolution, particularly as climate and land use change may affect flood frequency and intensity in many environments (e.g. Hunt, 2002, Milly et al., 2002, Pelletier et al., 2015; East and Sankey, 2020). Field studies of tracer transport have generally been restricted to timescales either relatively short (seconds to hours) or relatively long (positions before and after floods, up to decades) (e.g., Nikora et al., 2002; Haschenburger, 2013; Philips et al., 2013; Bradley, 2017). Few field-based studies have been able to quantify transport statistics during floods and span a wide range of timescales in one data set (e.g., McNamara and Borden, 2004; Olinde and Johnson, 2015; Habersack, 2001).

Statistical distributions of grain movements and rests control particle advection and diffusion through river networks (e.g., Einstein, 1937; Sayre and Hubbell, 1965). Bedload diffusion can be characterized in terms of the variance (σ_x^2) of particle displacements in the downstream (x) direction over a given time interval (t), such that $\sigma_x^2 \propto t^\gamma$. Normal (Fickian) diffusion occurs when variance increases linearly with time ($\gamma = 1$). Anomalous diffusion ($\gamma \neq 1$) can be further categorized into subdiffusion ($\gamma < 1$) and superdiffusion ($\gamma > 1$) (Weeks and Swinney, 1998; Martin et al., 2012). Anomalous diffusion indicates that nonlocal factors—

variables that are not only functions of that particular location and time but also depend on upstream-integrated effects--influence local transport (e.g., Foufoula-Georgiou and Passalacqua, 2013), including upstream watershed-dependent sediment supply and discharge, spatial variations in scour and fill, and grain size sorting. Nonlocality affects the accuracy of flux measurements over different averaging timescales, how clasts advect and disperse, and how environmental perturbations propagate through watersheds (e.g., Ganti et al. 2010, Martin et al 2012, Zhang et al., 2012). Mechanistically, transport processes that influence the degree to which particle hop and rest durations follow thin-tailed or heavy-tailed distributions can control whether diffusion is normal or anomalous (e.g., Weeks and Swinney, 1998; Nikora et al., 2002, Schumer et al., 2009, Zhang et al., 2012; Voepel et al., 2013; Martin et al., 2012; Martin et al., 2014; Fan et al., 2016, Bradley et al., 2010).

At least three distinct diffusion regimes have been interpreted as functions of timescale (e.g., Nikora et al., 2002), although Pierce and Hassan (2020) note that these diffusion ranges "are not resolved by any one data set". Contrasting diffusion behaviors have been interpreted for long ("global") timescales, including subdiffusion (Nikora et al., 2002; Cecchetto et al., 2018), normal diffusion (Zhang et al., 2012;, Voepel et al., 2013; Hassan et al., 2013; Haschenburger, 2013), and superdiffusion (Bradley et al., 2010, Bradley, 2017; Martin et al., 2012, Philips et al. 2013, Martin et al. 2014; Olinde and Johnson, 2015). While Nikora et al. (2002) hypothesized that flow intensity may also affect bedload diffusion, little previous work has explored this dependence. Using flume experiments, Heyman et al. (2013) and Liu et al. (2019) generally found that lower shear stresses corresponded to heavier-tailed rest time distributions.

Accelerometer-embedded smartrocks allow us to precisely measure the timing and durations of both motions and rests during a natural snowmelt flood. Pretzlav et al. (2020) use new smartrock data from Halfmoon Creek, Colorado to calculate bedload hysteresis and evolving thresholds of motion. In the present work, we analyze these data to explore different questions: How do rest durations scale over > 5 orders of temporal magnitude, and what do these distributions imply about bedload diffusion? Is rest time scaling independent of sediment transport intensity, or does it vary with hydrological forcing? Does cyclicity in flood discharge influence rest time distributions?

2. Field Site

Halfmoon Creek, Colorado, USA is well characterized by previous bedload transport work (Torizzo and Pitlick, 2004, Mueller and Pitlick, 2005; Bradley and Tucker, 2012; Bradley, 2017; Bunte and Swingle, 2005). Pretzlav et al. (2020) give details of our study reach and methods. Channel reach width is ≈7 m, depth from thalweg to banks ~1 m, and slope ~0.5%. Bed surface median grain diameter varied spatially between D_{50}≈6-13 cm in our reach, with D_{84}≈29 cm. USGS gaging station 07083000 is ≈1.5 km downstream. The 2015 snowmelt flood had a peak discharge of 11.5 m^3/s and a 10-year recurrence interval (Pretzlav et al., 2020). Pressure transducers monitored flow depth (h) in the reach, which was used to calculate shear stress $\tau = \rho g h S$ and Shields stress $\tau^* = \tau/(\rho_s - \rho)gD$, where ρ and ρ_s are water (1000 kg/m^3) and sediment (2650 kg/m^3) density, g is gravitational acceleration (9.81 m/s^2), S is reach slope, and D is the intermediate tracer diameter (7.2 cm, roughly bed D_{50}).

"Smartrock" cobbles were designed to infer the precise timing and duration of grain movements at high temporal resolutions. Custom high-density nylon tracer housings formed triaxial ellipsoids with axis diameters 7.2, 12.0 and 6.4 cm. Each smartrock contained a sensor (made by Gulf Coast Data Concepts LLC) which measured acceleration on 3 orthogonal axes ($\pm$2g), gyroscope rotation rate ($\pm$ 2000 degrees / second), and magnetometer compass direction ($\pm$ 1200 μT) using an InvenSense 9150 9-axis inertial measurement unit (IMU). Accelerometer and gyroscope data were collected at 10 Hz and used to calculate when individual motions started and ended. Pretzlav et al. (2020) describe the algorithm we developed that accurately measures motions and rests ≥2 s in duration.

Thirty-three tracers were deployed May 13, 2015, in the same location as Bradley and Tucker (2012), following their protocol of replacing a similarly-sized surface grain with a tracer to reduce enhanced mobility during initial motions. 27 tracers were recovered in fall 2015 when flow was low, although 6 of those sensors failed to record data. Because only 4 recovered tracers were buried, our data are likely biased towards surface grains. From the start of transport on June 3, individual tracers logged data for 2-28 days, limited by battery life. Our analysis uses all 15,536 movements from 21 tracers, detected over 28 days of diurnal hydrographs for which the entire flow was above threshold (Pretzlav et al., 2020). Hop durations are calculated from the start and end times of a given motion. Rest durations are calculated from the end of the last motion to the beginning of the next entrainment.

3. Scaling Methods

A distribution of tracer rest durations (t_d) is heavy-tailed when power law tail exponent $\alpha < 2$ for exceedance probability (*P*):

$$P(t_d > t) \propto t^{-\alpha} \qquad (1)$$

where t is a given time interval. Thin-tailed distributions (such as exponential functions; Figure 1a) have $\alpha \geq 2$ (e.g. Hassan et al., 2013). Following previous work, we assume that t_d are power-law distributed, with different tail exponents expected over different timescales (e.g., Nikora et al., 2002; Pierce and Hassan, 2020). We calculate α for rest time distributions from the entire 28-day record, using the Hill estimator of Nuyts (2010) which avoids bias in α estimates from only fitting a range of data within a given distribution. To objectively determine scaling breaks we apply the method of Clauset et al. (2009), which uses the Kolmogorov-Smirnov goodness of fit statistic (*KS*) to quantify how well different ranges of t_d are fit by power-law distributions. Scaling breaks are chosen at local *KS* minima, because lower *KS* values indicate that a given scaling break leads to a better power-law fit to that range of data (Figure 1b; see Supporting Information Text S2 for details). 95% confidence intervals are estimated using the bootstrap approach of Clauset et al. (2009), which involves subsampling t_d and calculating variability in repeated α estimates (Figure 1c).

Truncated and exponentially-tempered Pareto distributions can also fit our rest time data. Data collection methods that prevent larger values from being included in a given distribution can bias exponent estimates to lighter-tailed values, appearing as a "rollover" in exceedance probabilities at longer rest durations (Figure 1d). A Truncated Pareto distribution characterizes power-law behavior when there is a fixed upper limit in a data set (i.e., a single maximum measurable rest duration) (Aban et al., 2006; Bradley, 2017):

$$P(t_r > t) = \frac{t_o^{a_{tr}}\left(t^{-a_{tr}} - b^{-a_{tr}}\right)}{1-\left(t_o/b\right)^{a_{tr}}} \qquad \text{for } t_o < t < b,\ a_{tr} > 0 \quad (2)$$

where a_{tr} is the power-law tail exponent (comparable to α in Equation 1), truncation parameter b is the upper bound (i.e. maximum duration) that could be present in distribution t, and t_o is the minimum duration fit by the function. In principle, Equation (2) enables a_{tr} to be determined without truncation bias, as applied by Bradley (2017) for tracers over longer timescales in Halfmoon Creek.

Zhang et al. (2012), Voepel et al. (2013), and Hassan et al. (2013) argued that diffusion transitions from anomalous to normal as timescales increase to be very long, suggesting that rest time distributions should gradually become thin-tailed. To explore whether our data are consistent with this behavior, we also fit exponentially-tempered Pareto distributions, which gradually transition from power-law scaling at shorter timescales to thin-tailed exponential at longer timescales (Meerschaert et al., 2012):

$$P(t_r > t) = \left(t_o^{a_{et}} e^{ct_o}\right) t^{-a_{et}} e^{-ct} \qquad \text{for } t > t_o \qquad (3)$$

where power-law exponent a_{et} is comparable to α and a_{tr} in Equations (1) and (2), and c characterizes the exponential decay. Truncated and exponentially-tempered Pareto distributions can often fit the same data because both gradually transition to thin-tailed distributions at longer timescales, and “if the practitioner believes that a fixed upper bound is reasonable, then the truncated Pareto is suitable” (Meerschaert et al., 2012). In contrast, a variety of physical mechanisms (including but not limited to truncation) could result in data following an exponentially-tempered Pareto distribution, making it less diagnostic of underlying causes of observed scaling. We fit Equations (2) and (3) to rest-time distributions using Matlab nonlinear curve fitting (Figure 1d).

We also calculate separate rest time exponents for daily flood events 1-22 (Figure 2). Events 23-28 did not have sufficient numbers of rests to meaningfully constrain separate tail distributions following Clauset et al. (2009) methods; 99.7% of movements occurred before event 23. Rest distributions for all events 1-28 are shown in Supporting Information (Figure S2, S3). Rests were apportioned to each daily hydrograph (defined from discharge minimum to discharge minimum the following day; Figure 2g), with rest times truncated at the boundaries of each event. For example, if a tracer came to rest during event 4, and remained at rest until event

5, the rest was apportioned between each event. Diurnal rests cannot be longer than the diurnal cycle.

The control of bedload rest and hop statistics on anomalous diffusion has previously been inferred using the asymmetric random walk model of Weeks and Swinney (1998) (e.g., Martin et al., 2012, Olinde and Johnson, 2015; Bradley, 2017). Under thin-tailed hop durations (Figure 1b), diffusion exponent γ (i.e., $\sigma_x^2 \propto t^\gamma$) is a function of rest time tail exponent α:

$$\gamma = \begin{cases} 2\alpha, & 0 < \alpha \leq 1 \\ 3-\alpha, & 1 < \alpha < 2 \end{cases} \quad (4)$$

Fan et al. (2016) modeled bedload rests and hops and found diffusion consistent with Equation 4, supporting its use. Finally, Nikora et al. (2002) proposed that bedload diffusion scaling changed over different nondimensional timescales (t^*):

$$t^* = \frac{tu_\tau}{D} \quad (5)$$

where shear velocity $u_\tau = \sqrt{\tau/\rho}$.

4. Results

Hop durations ≥2 seconds follow a thin-tailed exponential distribution (Figure 1a), justifying the use of Equation 4, and consistent with laboratory experiments including Martin et al. (2012), Roseberry et al. (2012), and Liu et al. (2019).

Table 1 gives rest time exponent fits, calculated diffusion exponents, nondimensional timescales (Equations 1-5), and comparisons to previous field and experimental work. The *KS* minimum indicates that the strongest scaling break occurs at 12.5 (11.8-23.6) minutes, with additional scaling breaks suggested by local minima at 7 s (possible range 5.9-7.1 s) and 12.3 (11.8-12.9) hours (Figure 1b; Supporting Information; Clauset et al., 2009). Local *KS* minima >12.3 hours (most notably at ≈2.17×10^5 s, or ≈2.5 days) are not interpreted as additional breaks because α estimates are within uncertainty of each other for minima >12.3 hours, in part because the relatively small number of long rests give large α uncertainties (Clauset et al., 2009). Transitions between scaling regimes appear gradual (Figure 1c).

Rests between 7 s and 12.5 min follow α_1=0.28±0.02 (±95% confidence intervals). The numeric subscript on α simply indicates an Equation (1) fit to a particular timespan of the data, with α_1 representing 7 s-12.5 min (Figure 1c). For 12.5 min < t_r < 12.0 hours, α_2=0.62±0.05. For rests ≥12.3 hours, α_3=1.26±0.30 (the longest individual rest in our data is 12.24 days). From Equation (4) these heavy-tailed exponents correspond to γ_1=0.56±0.04, γ_2=1.24±0.1, and γ_3 =1.74 (1.44-2), suggesting a transition from subdiffusion (γ<1) to superdiffusion (γ>1) with increasing timescale (Table 1).

Rests can also be well fit by both truncated Pareto and exponentially-tempered Pareto distributions (Equations 2 and 3; Figure 1d). For t_r>12.5 min, a_{tr}=0.59±0.04 and a_{et}=0.60±0.03, within uncertainty of α_2=0.62±0.05. For t_r>12.3 hours, a_{tr}=1.0±0.25 and a_{et}=0.98±0.29 (Table 1). While within uncertainty of a_{tr} and a_{et} for t_r>12.3 hours, the higher value of α_3=1.26±0.30 may indicate bias by truncation of larger rest times.

Figure 1c compares smartrock rest times from Reynolds Creek, Idaho (Olinde and Johnson, 2015). For $t_r \geq$ 20 minutes, they reported α=0.67±0.11 using a different α estimation method. Using Nuyts (2010) and Clauset et al. (2009) methods for fitting Equation (1) we find α=0.73±0.14, within uncertainty of Halfmoon Creek α_2 (0.62±0.05; 12.5 min ≤ t_r ≤ 12.0 hr). A lack of rollover at longer rest times indicates that truncation or tempering effects are not evident in the Olinde and Johnson (2015) data.

By separately fitting rests for each daily hydrograph, Figure 2 demonstrates that rest time scaling varies systematically with shear stress over timescales from 7 s to 24 hours. Using short-duration scaling breaks from the seasonal dataset (Figure 1b), rests 7 s < t_r < 12.5 min were fit using Equation (1), while rests 12.5 min < t_r < 24 hours used Equation (2) to account for truncation (b=24 hours for this daily analysis). Exponents increase with Shields stress τ^* (Figure 2a,d), but are more strongly correlated with transport stage τ^*/τ^*_{cr} (Figure 2b,e). As calculated by Pretzlav et al. (2020), τ^*_{cr} evolved with daily floods and so transport stage reflects changes in both τ^* and τ^*_{cr}. In contrast, cumulative discharge explains little of the variability in rest scaling (Figure 2c,f), which we plot to evaluate whether changes in daily rest time scaling dominantly reflect clasts being progressively worked into the bed during the overall snowmelt flood.

5. **Discussion**

5.1 Scaling over seconds to minutes

Because hop durations are thin-tailed, dispersion exponents (γ) should primarily depend on rest time scaling (Equation 4; Weeks and Swinney, 1998). Our shortest duration scaling regime (γ_1=0.56±0.04 for 7 s ≤ t_r ≤ 12.5 min) predicts subdiffusion over nondimensional timescales 22<t^*<2400 (Equation 5, D=7.2 cm, average u_τ =0.23 m/s; Pretzlav et al., 2020). These results are consistent with previous work of Cecchetto et al. (2018; γ≈0.6 for 100< t^*<2000) and Nikora et al. (2002; γ≈0.66 for 15< t^*<2000) (Table 1).

Mechanistically, over short timescales bedload transport is strongly influenced by turbulence, including coherent flow structures such as "sweeps" (e.g., Drake et al., 1988; Roseberry et al., 2012). Spatial and temporal correlations in fluid velocity fields can cause anomalous diffusion in physical systems (Bouchaud and Georges, 1990; Weeks et al., 1996). Heyman et al. (2013) conducted flume experiments with rest durations from ≈0.1-4.5 s (1.2<t*<61), and found that rest distributions varied with shear stress. They hypothesized that turbulent sweeps transported a higher proportion of sediment at lower τ* (resulting in heavier-tailed rest distributions due to longer rests between sweeps), while more grains moved independently from sweeps at higher τ* (resulting in less heavy-tailed rest distributions). We hypothesize that temporal velocity correlations may similarly explain our rest time τ* dependence over 7 s ≤ t_r ≤ 12.5 minutes (22<t^*<2400) (Figure 2a,b). In a gravel-bed pool-riffle channel, Marquis and Roy (2011) found that turbulence was clustered or "imbricated" and caused velocities to accelerate and decelerate, or "pulse", over timescales from several seconds to ≈10 minutes that bridge variability in turbulence and discharge. Mechanistically, a particle will be more likely to have last moved when flow velocities were higher. The probability of high velocities will increase with both shear stress and over the timescales of sweeps and pulsing. A reduced likelihood that clasts remain at rest would cause α to progressively increase with shear stress (i.e., increasing α corresponds to fewer long rests). Our hydraulic data (gaging station discharge at 15 minute intervals) are insufficient to evaluate these dependencies.

5.2 Scaling over minutes to hours

The superdiffusive scaling suggested by our season-averaged intermediate regime (γ_2 =1.24±0.1 for 2400<t*<1.4×10^5) are similar to Olinde and Johnson (2015) (γ =1.46±0.28 for 2700 <t*<2×10^6; Figure 1c) and other previous field and experimental work (Table 1). Pierce and Hassan (2020) proposed a random-walk model that predicted changes in diffusion scaling with timescale; their "intermediate" timescale scaling $\gamma \approx 1$ is similar to our results over minutes to hours. Mechanistically, motions and rests (with negligible burial) control diffusion over intermediate timescales in their model.

Combining all rests from the month-long flood record (Figure 1c,d) masks the observation that rest time scaling varies systematically with daily hydraulic forcing (Figure 2a-f). For daily flood hydrographs, scaling exponents increase with hydrograph-averaged Shields stress and transport stage. Olinde and Johnson (2015) similarly found higher α in their largest flood compared to smaller prior events, although their data collection methods could not quantify shear stress dependence. Singh et al. (2009) found that statistical measures of bedload flux variability ("roughness" and "intermittency") decreased as τ^*/τ^*_{cr} increased. We interpret that fewer rests are exceptionally long as τ^*/τ^*_{cr} increases because transport rates become less intermittent. This results in rest time exponents that become less heavy (i.e. lower values of α).

Wilcock and McArdell (1993) interpreted that full mobility of surface GSDs occurs in gravel-bed channels when $\tau^* \approx 2\tau^*_{cr}$. Figure 2 allows us to predict the flow conditions at which α =2 and diffusion should transition from anomalous to normal (γ =1). Assuming that the linear regressions can be extrapolated to higher τ^*/τ^*_{cr}, rests>12.5 min and 7 s<t_r<12.5 min similarly predict that α=2 at τ^*/τ^*_{cr} ≈2.1-2.3, with a 95% confidence interval between τ^*/τ^*_{cr} ≈1.8 and 3.4. Future work could test the quantitative hypothesis that coarse bedload exhibits normal diffusion during floods with transport at or near full mobility ($\tau^* \gtrsim 2\tau^*_{cr}$).

5.3 Scaling over hours to weeks

Our season-averaged rest times >12.3 hours can be empirically fit in multiple ways (Figure 1c,d). Because our statistics are not sufficient to distinguish between these, we present several contrasting interpretations of diffusion. First, we interpret that the scaling break found using the Clauset et al. (2009) method at 12.3 hr is real, rather than an artifact from rest time variability combined with gradual truncation (Figure 1b-d; see Supporting Information for scaling break details). For our rest durations 12.3 hrs < t_r < 12.24 days, Equations (1) and (4) suggest superdiffusion (γ_3=1.44-2 at 95% confidence, Table 1). We can account for possible truncation effects for rests >12.3 hrs using the truncated or exponentially-tempered Pareto distributions, which suggest comparable superdiffusive behavior (γ=1.5-2 or 1.38-2, respectively). This scaling is consistent with Phillips et al et al. (2013), who measured $\gamma = 1.88$ over multiple natural floods spanning similar timescales (Table 1).

Because truncated and exponentially-tempered distribution can fit rests >12.5 minutes, a second possible interpretation is that these data reflect gradual truncation combined with noise, with no scaling break at 12.3 hours (Figure 1d). In this case, the “true” scaling exponents (a_{tr}=0.59±0.04 or a_{et} =0.6±0.03) suggest γ=1.2±0.08, consistent with γ_2=1.24±0.1, with γ=1.46±0.28 for Reynolds Creek, and with γ=1.34 measured by Bradley (2017) for Halfmoon Creek over multiple years (Table 1). The range of best-fit truncation times (*b* in Equation 2; $8.6\times10^5 \pm 2.9\times10^5$ s and $6.8\times10^5 \pm 3.2\times10^5$ s, Figure 1d) spans 4-13 days, shorter than the total sampling duration. Individual smartrock batteries failed at different times (between daily hydrographs 3 and 28; Pretzlav et al., 2020), giving a distribution of truncation times. This may explain why the rollover appears more gradual than the truncated Pareto distribution, which assumes a single truncation value.

Third, a final possible interpretation of our data is that the gradual rollover at longer rest durations is real and not just an artifact of truncation. In this scenario, the exponentially-tempered Pareto fits could indicate a transition to thin-tailed rest distributions and normal diffusion (γ=1) over longer timescales, as has been suggested by Hassan et al. (2013) over seasons to decades. We emphasize contrasting statistically-supported interpretations of our data to motivate future work that can distinguish between these possibilities at longer timescales, and because some previous work might be affected by truncation and/or by potentially large uncertainties on exponents calculated from small numbers of tail distribution measurements (e.g., Clauset et al., 2009; Supporting Information Text S1).

Mechanistically, bed scour and fill may provide a nonunique but physically plausible explanation for a transition from superdiffusion to normal diffusion, based on modeling by Voepel et al. (2013). However, models by Martin et al. (2014) and Pierce and Hassan (2020) predicted that strong superdiffusion (with $\gamma\approx2$) should persist over these longer timescales of intermittent burial, consistent with our possible interpretation of $\gamma\approx1.4$-2 for $t_r>12.3$ hr. Our data may not fully capture effects of burial and exhumation on rest times, as 23 out of 27 recovered tracers were found on the bed surface (Pretzlav et al., 2020). Perhaps grain interlocking on the bed surface (Yager et al., 2018), or grain trapping in deep surface pockets enabled by a broad grain size distribution, can cause rest time scaling comparable to local burial and scour.

Finally, we hypothesize that discharge cyclicity may cause the possible ≈12 hr scaling break in Halfmoon Creek rests (Figure 1b, c). Importantly, a similar break is not observed in Reynolds Creek (Olinde and Johnson, 2015), even though the smartrock methods and flood durations above threshold were similar (Figure 1c). Figure 2g-j shows that daily hydrograph cyclicity causes local peaks in power spectral density at 12 and 24 hours in both channels, but peaks are an order of magnitude lower in Reynolds Creek because the diurnal hydrographs are less sinusoidal and more variable in duration. We hypothesize that the ≈12 hr Halfmoon break occurs because discharge cyclicity reduces the probability of clasts remaining at rest for longer than the duration of one rising or falling limb. In contrast, we hypothesize that Reynolds Creek rests do not show a corresponding scaling break because power is more distributed over a range of periods, reflecting less cyclicity in the shear stresses that drive bedload transport (e.g., Bouchaud and Georges, 1990). Although the Halfmoon spectral density is higher at 24 hr, perhaps the scaling break occurred at 12 rather than 24 hr simply because the shorter duration cyclicity overprints the 24 hr signal. Note also that another Halfmoon spectral peak at $\approx2.12\times10^5$ s (2.5 days) is very similar in rest duration to a minor *KS* minima at $\approx2.17\times10^5$ s (Figure 1b), suggesting again that hydrograph cyclicity might be expressed in rest time distributions. Regardless, our analyses suggest that the effects of flow intensity and cyclicity on anomalous diffusion across timescales warrant further study.

6. Conclusions

Consistent with previous experimental work, motion sensor-embedded tracers indicate an exponential distribution of hop times during a natural flood. Our rest time scaling predicts subdiffusion over timescales from 7 seconds to 12.5 minutes, and superdiffusion for rest durations from 12.5 minutes to 12.3 hours. For durations >12.3 hr, our data can be nonuniquely fit by heavy-tailed power law or truncated Pareto distributions which predict superdiffusion, but also by an exponentially-tempered Pareto distribution which suggests a gradual transition to normal (Fickian) diffusion at even longer timescales.

Daily rest time scaling varies systematically with shear stress, indicating a transition from subdiffusion to superdiffusion with increasing transport capacity. We hypothesize that a rest time scaling change at ≈12 hours is influenced by the cyclicity of daily snowmelt flood hydrographs.

Figure Captions

Figure 1. (a) Hop duration exceedance probabilities with the best-fit exponential to hops >2 seconds. (b) Scaling breaks indicated by local minima in Kolmogorov-Smirnov statistic, following method of Clauset et al. (2009). (c) Rest duration exceedance probabilities, with Equation (1) exponents for Halfmoon and Reynolds Creek. (d) Halfmoon Creek rest times > 12.5 minutes and >12.3 hours, each fit with truncated and exponentially-tempered Pareto distributions (R^2>0.99 for each fit).

Figure 2. (a-f) For daily hydrographs, rest duration tail exponents systematically increase with Shields stress (a,d) and transport stage (b,e) but minimally correlate with cumulative discharge (c,f). Error bars and regression uncertainties represent 95% confidence intervals (2σ); regressions were weighted by $1/\sigma^2$ for each data point. Outlier event 1 was not included in regressions because grains started in less stable positions (Pretzlav et al., 2020). For d-f, b=24 hours; t_o=12.5 min (Equation 2). (g) Hydrographs during motion tracer sampling for Halfmoon Creek, Colorado, showing sequential floods 1-28, and (h) 2012 flood, Reynolds Creek, Idaho, recurrence interval 4.5 years (Olinde and Johnson, 2015). (i, j). Power spectral density for the Halfmoon and Reynolds Creek hydrographs, calculated using Matlab “periodogram” function. For 12 hour and 24 hr periods, power is an order of magnitude higher for Halfmoon than for

Reynolds Creek. The strongest peak in spectral density corresponds to the length of the spring floods.

Acknowledgements

This work was funded by the National Science Foundation (EAR 1053508 to JPLJ) and by The University of Texas at Austin Jackson School of Geosciences. Tail exponent and uncertainty estimation used modifications of Matlab code (plfit.m, plvar.m) from A. Clauset (http://tuvalu.santafe.edu/~aaronc/powerlaws/). If the manuscript is accepted, data will be available in a data archive following GRL guidelines. For now spreadsheets of data are included with the submission.

References

Aban, I., Meerschaert, M., & Panorska, A. (2006), Parameter estimation for the truncated Pareto distribution. Journal of the American Statistical Association, 101, 270–277. https://doi.org/10.1198/016214505000000411

Bouchaud, J-P, and A. Georges (1990), Anomalous diffusion in disordered media: Statistical mechanisms, models and physical applications. Physics Reports, Volume 195, Issues 4–5, Pages 127-293, https://doi.org/10.1016/0370-1573(90)90099-N.

Bradley, D.N., Tucker, G.E., and Benson, D.A. (2010), Fractional dispersion in a sand bed river: Journal of Geophysical Research, v. 115, p. 1–20, doi: 10.1029/2009JF001268.

Bradley, D.N, and Tucker, G.E. (2012), Measuring gravel transport and dispersion in a mountain river using passive radio tracers: Earth Surface Processes and Landforms, v. 37, no. 10, p. 1034–1045, doi: 10.1002/esp.3223.

Bradley, D. N. (2017). Direct observation of heavy-tailed storage times of bed load tracer particles causing anomalous superdiffusion. Geophysical Research Letters, 44, 12,227–12,235. https://doi.org/10.1002/2017GL075045

Bunte, K., K. W. Swingle (2005), Using bedload traps at Halfmoon Creek, 2004: Transport rates, spatial variability of gravel transport, and long nets. Report submitted to the Stream Systems

Technology Center, USDA Forest Service, Rocky Mountain Research Station, Fort Collins, CO. 116 pp.

Cecchetto, M., Tregnaghi, M., Bottacin-Busolin, A., Tait, S. J., Cotterle, L., & Marion, A. (2018), Diffusive regimes of the motion of bed load particles in open channel flows at low transport stages. Water Resources Research, 54, 8674–8691. https://doi.org/10.1029/2018WR022885

Clauset, A., C.R. Shalizi, and M.E.J. Newman (2009), "Power-law distributions in empirical data" *SIAM Review* 51(4), 661-703 (2009). (arXiv:0706.1062, doi:10.1137/070710111)

Drake, T., Shreve, R., Dietrich, W., Whiting, P., & Leopold, L. (1988), Bedload transport of fine gravel observed by motion-picture photography. *Journal of Fluid Mechanics, 192*, 193-217. doi:10.1017/S0022112088001831

East, A. E., & Sankey, J. B. (2020), Geomorphic and sedimentary effects of modern climate change: current and anticipated future conditions in the western United States. *Reviews of Geophysics*, 58, e2019RG000692. https://doi.org/10.1029/2019RG000692

Einstein, H. A. (1937), Bed load transport as a probability problem. In H. W. Shen (Ed.), *Sedimentation*. Fort Collins, Colo. 1972: Appendix C.

Fan, N., A. Singh, M. Guala, E. Foufoula-Georgiou, and B. Wu (2016), Exploring a semimechanistic episodic Langevin model for bed load transport: Emergence of normal and anomalous advection and diffusion regimes, Water Resour. Res., 52, 2789–2801, doi:10.1002/2015WR018023.

Foufoula-Georgiou, E., Passalacqua, P. (2013), Nonlocal transport theories in geomorphology: mathematical modeling of broad scales of motion. In: Shroder, J. (Editor in Chief), Baas, A.C.W. (Ed.), Treatise on Geomorphology. Academic Press, San Diego, CA, vol. 2, Quantitative Modeling of Geomorphology, pp. 98–116. http://dx.doi.org/10.1016/B978-0-12-374739-6.00032-4

Ganti, V., M. M. Meerschaert, E. Foufoula-Georgiou, E. Viparelli, and G. Parker (2010), Normal and anomalous diffusion of gravel tracer particles in rivers, J. Geophys. Res., 115, F00A12, doi:10.1029/2008JF001222.

Habersack, H. M. (2001), Radio-tracking gravel particles in a large braided river in New Zealand: A field test of the stochastic theory of bed load transport proposed by Einstein, Hydrol. Processes, 15(3), 377–391, doi:10.1002/hyp.147.

Haschenburger, J.K. (2013), Tracing river gravels: Insights into dispersion from a long-term field experiment. Geomorphology, Volume 200, Pages 121-131, https://doi.org/10.1016/j.geomorph.2013.03.033.

Hassan, M. a., Voepel, H., Schumer, R., Parker, G., and Fraccarollo, L. (2013), Displacement characteristics of coarse fluvial bed sediment: Journal of Geophysical Research: Earth Surface, v. 118, no. February 2012, p. n/a–n/a, doi: 10.1029/2012JF002374.

Heyman, J., F. Mettra, H. B. Ma, and C. Ancey (2013), Statistics of bedload transport over steep slopes: Separation of time scales and collective motion, Geophys. Res. Lett. 40, 128–133, doi: 10.1029/2012GL054280.

Hunt, J.C.R. (2002), Floods in a changing climate: a review.: Philosophical transactions. Series A, Mathematical, physical, and engineering sciences, v. 360, no. 1796, p. 1531–43, doi: 10.1098/rsta.2002.1016.

Liu, M. X., Pelosi, A., & Guala, M. (2019). A statistical description of particle motion and rest regimes in open-channel flows under low bedload transport. *Journal of Geophysical Research: Earth Surface*, *124*, 2666 2688. https://doi.org/10.1029/2019JF005140

Marquis G.A and A.G. Roy (2011), Bridging the gap between turbulence and larger scales of flow motions in rivers. Earth Surf. Process. Landforms 36, 563–568, DOI: 10.1002/esp.2131

Martin, R.L., Jerolmack, D.J., and Schumer, R. (2012), The physical basis for anomalous diffusion in bed load transport: Journal of Geophysical Research, v. 117, no. F1, p. F01018, doi: 10.1029/2011JF002075.

Martin, R.L., Purohit, P.K., and Jerolmack, D.J. (2014), Sedimentary bed evolution as a mean-reverting random walk: Implications for tracer statistics: Geophysical Research Letters, , no. May, p. n/a–n/a, doi: 10.1002/2014GL060525.

McNamara, J. P., and C. Borden (2004), Observations on the movement of coarse gravel using implanted motion-sensing radio transmitters, Hydrol. Processes, 18(10), 1871–1884, doi:10.1002/hyp.1453.

Meerschaert, M. M., P. Roy, and Q. Shao (2012), Parameter estimation for tempered power law distributions, Commun. Stat. Theory Methods, 41(10), 1839–1856, doi: 10.1080/03610926.2011.552828

Milly, P.C.D., Wetherald, R.T., Dunne, K. a, and Delworth, T.L. (2002), Increasing risk of great floods in a changing climate: Nature, v. 415, no. 6871, p. 514–517, doi: 10.1038/415514a.

Mueller, E. R., and Pitlick, J. (2005), Morphologically based model of bed load transport capacity in a headwater stream, *J. Geophys. Res.*, 110, F02016, doi:10.1029/2003JF000117.

Nikora, V., Habersack, H., Huber, T., and McEwan, I. (2002), On bed particle diffusion in gravel bed flows under weak bed load transport: Water Resources Research, v. 38, no. 6, p. 17–1–17–9, doi: 10.1029/2001WR000513.

Nuyts, J. (2010), Inference about the tail of a distribution: Improvement on the Hill estimator, Int. J. Math. Math. Sci., 2010, 924013, doi:10.1155/2010/924013.

Olinde, L., and Johnson, J.P.L. (2015), Using RFID and accelerometer-embedded tracers to measure probabilities of bed load transport, step lengths, and rest times in a mountain stream: Water Resources Research, v. 51, no. 9, p. 7572–7589, doi: 10.1002/2014WR016120.

Pelletier, J.D., Brad Murray, A., Pierce, J.L., Bierman, P.R., Breshears, D.D., Crosby, B.T., Ellis, M., Foufoula-Georgiou, E., Heimsath, A.M., Houser, C., Lancaster, N., Marani, M., Merritts, D.J., Moore, L.J., et al. (2015), Forecasting the response of Earth's surface to future climatic and land use changes: A review of methods and research needs: Earth's Future, v. 3, no. 7, p. 220–251, doi: 10.1002/2014EF000290.

Phillips, C.B., Martin, R.L., and Jerolmack, D.J. (2013), Impulse framework for unsteady flows reveals superdiffusive bed load transport: Geophysical Research Letters, v. 40, no. 7, p. 1328–1333, doi: 10.1002/grl.50323.

Pierce, J. K., & Hassan, M. A. (2020). Back to Einstein: Burial-induced three-range diffusion in fluvial sediment transport. *Geophysical Research Letters*, *47*, e2020GL087440. https://doi.org/10.1029/2020GL087440

Pretzlav, K. L. G., Johnson, J. P. L., & Bradley, D. N. (2020). Smartrock transport in a mountain stream: Bedload hysteresis and changing thresholds of motion. *Water Resources Research*, *56*, e2020WR028150. https://doi.org/10.1029/2020WR028150

Roseberry, J. C., M.W. Schmeeckle, D. J. Furbish (2012), A probabilistic description of the bed load sediment flux: 2. Particle activity and motions, J Geophys. Res., 117, F03032, doi:10.1029/2012JF002353.

Sayre, W., and D. Hubbell (1965), Transport and dispersion of labeled bed material, North Loup River, Nebraska, U.S. Geol. Surv. Prof. Pap., 433-C, 48 pp.

Schumer, R., Meerschaert, M.M., and Baeumer, B. (2009), Fractional advection-dispersion equations for modeling transport at the Earth surface: Journal of Geophysical Research: Earth Surface, v. 114, no. 4, p. 1–15, doi: 10.1029/2008JF001246.

Singh, A., Fienberg, K., Jerolmack, D.J., Marr, J., and Foufoula-Georgiou, E. (2009), Experimental evidence for statistical scaling and intermittency in sediment transport rates: Journal of Geophysical Research, v. 114, no. F1, p. F01025, doi: 10.1029/2007JF000963.

Torizzo, M., & Pitlick, J. (2004). Magnitude-frequency of bed load transport in mountain streams in Colorado. Journal of Hydrology, 290(1-2), 137-151. doi:doi:10.1016/j.jhydrol.2003.12.001

Voepel, H., R. Schumer, and M. A. Hassan (2013), Sediment residence time distributions: Theory and application from bed elevation measurements, J. Geophys. Res. Earth Surf., 118, 2557–2567, doi:10.1002/jgrf.20151.

Weeks, E.R., Urbach, J.S., and Swinney, H.L. (1996), Anomalous diffusion in asymmetric random walks with a quasi-geostrophic flow example: Physica D: Nonlinear Phenomena, v. 97, no. 1-3, p. 291–310, doi: 10.1016/0167-2789(96)00082-6.

Weeks, E., and Swinney, H. (1998), Anomalous diffusion resulting from strongly asymmetric random walks: Physical Review E, v. 57, no. 5, p. 4915–4920, doi: 10.1103/PhysRevE.57.4915.

Wilcock, P.R., and B.W. McArdell (1993), Surface-based fractional transport rates: Mobilization thresholds and partial transport of a sand-gravel sediment, Water Resour. Res., 29, 1297-1312, https://doi.org/10.1029/92WR02748

Yager, E. M., Schmeeckle, M. W., & Badoux, A. (2018), Resistance is not futile: Grain resistance controls on observed critical Shields stress variations. Journal of Geophysical Research: Earth Surface, 123, 3308–3322. https://doi.org/10.1029/2018JF004817

Zhang, Y., M. M. Meerschaert, and A. I. Packman (2012), Linking fluvial bed sediment transport across scales, Geophys. Res. Lett., 39, L20404, doi:10.1029/2012GL053476.

Table 1: Comparison of field and experimental data

	Rest duration exponent (95% confidence intervals if reported)	***t** range (Equation 5)**	**Rest duration range (time above threshold)**	**Diffusion exponent γ** (95% confidence intervals if reported)	**Interpretation**	**Method**
Seconds to minutes						
This paper	$\alpha_1 = 0.28 \pm 0.02$	$22 < t^* < 2400$	$7\ s < t_r < 12.5$ min	$\gamma_1 = 0.56 \pm 0.04$†	subdiffusion	Power-law (Eq. 1)
Nikora et al., 2002	0.33	$200 < t^* < 2000$	$14\ s < t_r < 140$ s	0.66†	subdiffusion	Power-law (Eq. 1)
Cecchetto et al., 2018	0.3	$100 < t^* < 2000$	$7\ s < t_r < 140$ s	0.60†	subdiffusion	Power-law (Eq. 1)
Minutes to hours						
This paper	$\alpha_2 = 0.62 \pm 0.05$	$2400 < t^* < 1.4 \times 10^5$	12.5 min $< t_r <$ 12.3 hrs	$\gamma_2 = 1.24 \pm 0.1$†	superdiffusion	Power-law (Eq. 1)
This paper	$a_{tr} = 0.59 \pm 0.04$	$2400 < t^* < 3.4 \times 10^6$	12.5 min $< t_r <$ 12.24 days	1.18 ± 0.08†	superdiffusion	Truncated Pareto (Eq. 2)
This paper	$a_{et} = 0.60 \pm 0.03$	$2400 < t^* < 3.4 \times 10^6$	12.5 min $< t_r <$ 12.24 days	1.20 ± 0.06†	superdiffusion	Exp-temp. Pareto (Eq. 3)
Olinde & Johnson, 2015	0.73 ± 0.14	$2700 < t^* < 2 \times 10^6$	20 min $< t_r <$ 7.8 days	1.46 ± 0.28†	superdiffusion	Power-law (Eq. 1)
Martin et al., 2012	0.68, 0.85‡	$500 < t^* < 13000$	13 s $< t_r <$ 13 min	1.36, 1.70†	superdiffusion	Power-law (Eq. 1)
Hours to weeks						
This paper	$\alpha_3 = 1.26 \pm 0.30$	$1.4 \times 10^5 < t^* < 3.4 \times 10^6$	12.3 hrs $< t_r <$ 12.24 days	$\gamma_3 = 1.74$ (1.4 - 2.0)†	superdiffusion	Power-law (Eq. 1)
This paper	$a_{tr} = 1.00 \pm 0.25$	$1.4 \times 10^5 < t^* < 3.4 \times 10^6$	12.3 hrs $< t_r <$ 12.24 days	2 (1.5-2)†	superdiffusion	Truncated Pareto (Eq. 2)
This paper	$a_{et} = 0.98 \pm 0.29$	$1.4 \times 10^5 < t^* < 3.4 \times 10^6$	12.3 hrs $< t_r <$ 12.24 days	1.96 (1.38-2)†	superdiffusion	Exp-temp. Pareto (Eq. 3)
Bradley, 2017	$a_{tr} = 0.67$†	$6 \times 10^6 < t^* < 8 \times 10^7$	12 days $< t_r <$ 167 days	1.34	superdiffusion	Truncated Pareto (Eq. 2)
Phillips et al., 2013	0.94 or 1.12†	$5.4 \times 10^4 < t^* < 2.2 \times 10^6$	7 hrs $< t_r <$ 11 days	1.88	superdiffusion	Power-law (Eq. 1)

† Calculated using Equation (4)

‡ The two values are from two similar experiments

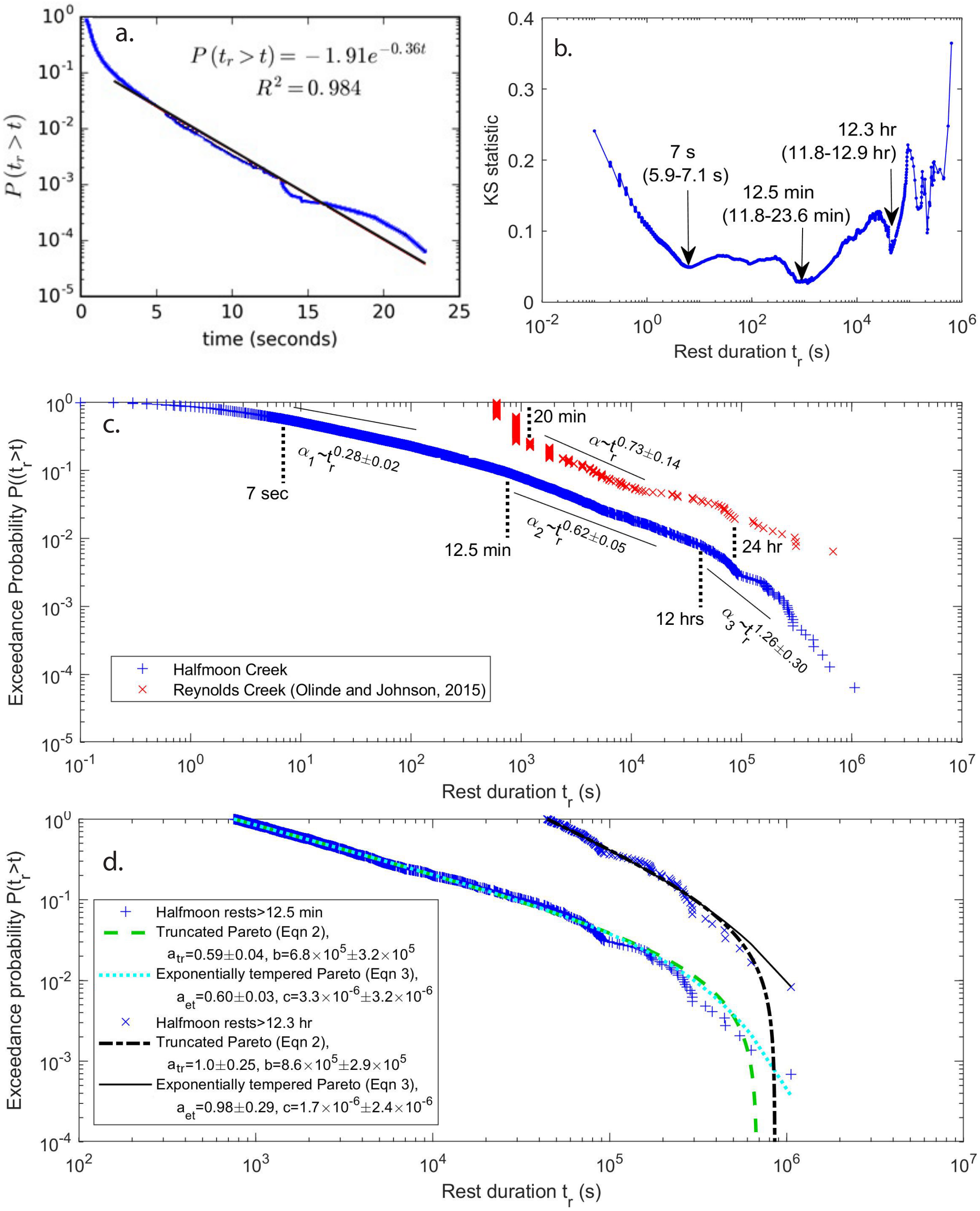

a.
$P(t_r > t) = -1.91e^{-0.36t}$
$R^2 = 0.984$
$P(t_r > t)$
time (seconds)
b.
KS statistic
7 s
(5.9-7.1 s)
12.5 min
(11.8-23.6 min)
12.3 hr
(11.8-12.9 hr)
Rest duration t_r (s)
c.
Exceedance Probability $P((t_r>t)$
20 min
α~$t_r^{0.73\pm0.14}$
α_1~$t_r^{0.28\pm0.02}$
7 sec
α_2~$t_r^{0.62\pm0.05}$
12.5 min
24 hr
12 hrs
α_3~$t_r^{1.26\pm0.30}$
Halfmoon Creek
Reynolds Creek (Olinde and Johnson, 2015)
Rest duration t_r (s)
d.
Exceedance probability $P(t_r>t)$
Halfmoon rests>12.5 min
Truncated Pareto (Eqn 2),
a_{tr}=0.59±0.04, b=6.8×10^5±3.2×10^5
Exponentially tempered Pareto (Eqn 3),
a_{et}=0.60±0.03, c=3.3×10^{-6}±3.2×10^{-6}
Halfmoon rests>12.3 hr
Truncated Pareto (Eqn 2),
a_{tr}=1.0±0.25, b=8.6×10^5±2.9×10^5
Exponentially tempered Pareto (Eqn 3),
a_{et}=0.98±0.29, c=1.7×10^{-6}±2.4×10^{-6}
Rest duration t_r (s)

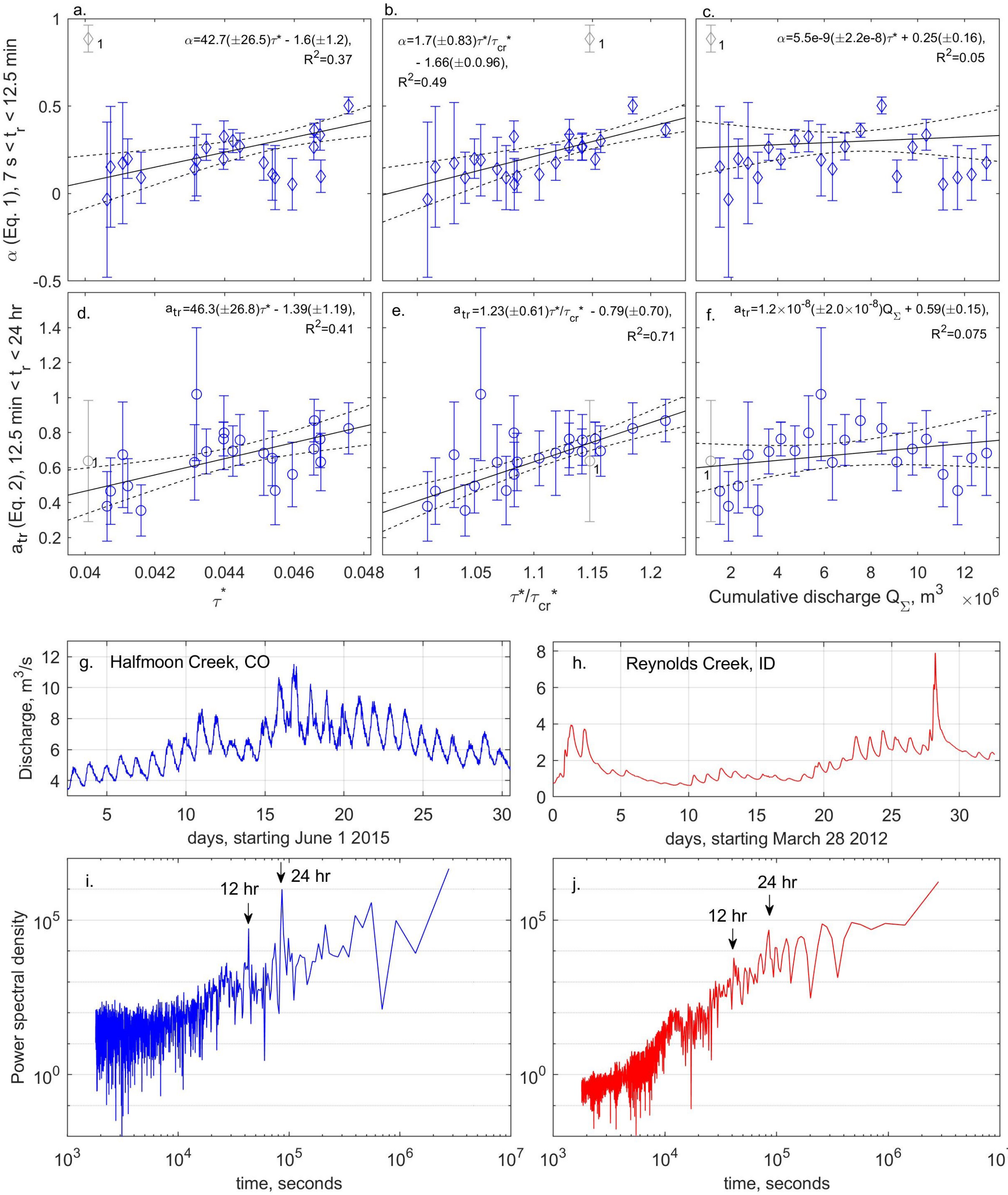
a.
b.
c.
d.
e.
f.
α=42.7(±26.5)τ* - 1.6(±1.2), R²=0.37
α=1.7(±0.83)τ*/τcr* - 1.66(±0.0.96), R²=0.49
α=5.5e-9(±2.2e-8)τ* + 0.25(±0.16), R²=0.05
atr=46.3(±26.8)τ* - 1.39(±1.19), R²=0.41
atr=1.23(±0.61)τ*/τcr* - 0.79(±0.70), R²=0.71
atr=1.2×10-8(±2.0×10-8)QΣ + 0.59(±0.15), R²=0.075
α (Eq. 1), 7 s < tr < 12.5 min
atr (Eq. 2), 12.5 min < tr < 24 hr
τ*
τ*/τcr*
Cumulative discharge QΣ, m3
g.
Halfmoon Creek, CO
h.
Reynolds Creek, ID
Discharge, m3/s
days, starting June 1 2015
days, starting March 28 2012
i.
j.
12 hr
24 hr
Power spectral density
time, seconds